# PARTIAL ADMISSION EFFECTS ON THE FLOW FIELD OF AN ORC TESLA TURBINE

Leonardo Pacini[1], Lorenzo Ciappi[1], Lorenzo Talluri[1]*, Daniele Fiaschi[1], Giampaolo Manfrida[1] and Jacek Smolka[2]

[1]Department of Industrial Engineering, Università degli Studi di Firenze,
Viale Morgagni 40-44, 50134 Florence, Italy
lorenzo.talluri@unifi.it

[2]Institute of Thermal Technology, Silesian University of Technology,
Konarskiego 22, Gliwice, Poland

*Corresponding Author

## ABSTRACT

Over recent years, Tesla turbine gained a renewed interest from the international scientific community, as it combines reliability, efficiency and low cost. These are key aspects for the success of an expander suitable for small-distributed energy systems; thus Tesla turbine could represent an attracting solution for the market.
The test case is a turbine with efficiency 29% for a 0.57 kW expander utilizing R1233zd(E) as working fluid. The three-dimensional fluid dynamics inside the stator, the stator-rotor gap and the rotor is determined by means of CFD analyses. The comprehensive evaluation of the set of the three regions is of paramount importance to determine the machine flow field, as it is significantly affected by the interactions amongst each component. In particular, the effects of discrete admission to the rotor are relevant in terms of flow field distortion, while the effects on the performance parameters (power and efficiency) are slighter. The performance results of the 3-D computational fluid dynamics are close to the ones of the 2-D in-house developed code, which assumes continuous admission to the rotor.
The results inside the rotor are shown in terms of velocity, pressure and temperature fields. Particular interest is focused on the distinctive shape of the temperature distribution inside the rotor, arising from the spiral trajectories of the fluid determined by the four admission nozzles.

## 1. INTRODUCTION

The research world is starting to evaluate the possibility of utilizing Tesla turbines for ORCs for distributed heat and power generation. This field of application is especially suitable for ORCs, because of their favourable fluid properties (low critical pressure and temperature and high molecular mass when compared to steam). Nonetheless, due to the low temperature of the resource, only low energy conversion rates are commonly achieved and the expander is a critical component, especially for micro power generation. Nowadays, the most widespread expanders in ORCs for micro power generation are volumetric expanders (Lemort and Legros, 2016; Dumont *et al.*, 2018), while dynamic expanders (turbines) are not the optimal choice for power values lower than 50 kW (Qiu *et al.*, 2011). Tesla turbine seems to be a promising competitor in the field of small power generation, thanks to its low cost, simple structure and reliability. Out of the many published works, four main lines of research stirred up a renovated interest in the Tesla turbine. The most extensive work was carried out by W. Rice, who analyzed the Tesla turbine, both developing an analytical 2-D model and through the realization of six different prototypes, tested with air as a working fluid (Rice, 1965). Another relevant line of research was developed by A. Guha and S. Sengupta. In their work, an upgraded analytical model was realized and compared to the CFD investigations (Guha and Sengupta, 2014). Furthermore, the realization of an experimental campaign on the air Tesla turbine was performed with the aim of depicting the main causes of inefficiency (Hoya and Guha, 2009). The third main line of research was the one headed by V.P.

Carey, who took over the work developed by W. Rice and further generalised the 2-D model, applying it also to applications in the Watt and sub-Watt power ranges (Carey, 2010; Krishnan *et al.*, 2013). A recent line of research is the one carried on by C. Schosser and M. Pfizner, who performed numerical and experimental analyses (Schosser *et al.*, 2014; Schosser and Pfitzner, 2015). The most significant outcome of their research was the visualisation and the assessment of the flow behaviour inside the Tesla turbine rotor working with air. Apart from these strongholds, several interesting spot research works were published. Out of the many publications, the ones of P. Lampart and Jedrzejewki (2011) and the ones from J. Song *et al.* (2017) and (2018) are worth mentioning as they investigated the possibility of utilising the Tesla turbine with organic fluids. Finally, the Sustainable Energy Research Group (SERG) of University of Florence contributed to the development of the state of the art of the Tesla turbine (Manfrida *et al.*, 2018; Talluri *et al.*, 2018), introducing advancements in the design and optimization of the machine for the use within ORCs, through the development of both 2-D and 3-D CFD models. Even though there are several analytical and numerical models present in literature, the assessment of the effects derived by the interaction between the admission nozzles and the rotor has not yet been fully explained. Therefore, the aim of this work is to assess the effects of the flow distortion at rotor inlet and highlight the influence of partial admission on the performance of the Tesla turbine.

## 2. METHODOLOGY

The Tesla turbine is a bladeless turbine, comprised of one or more nozzles that direct the working fluid as much tangential as possible at rotor inlet. The rotor is composed of several stacked parallel disks, assembled very close to each other, forming very tight gaps, enabling work exchange between the fluid and the disks through viscous effects. The fluid enters from the outer radius of the rotor, and depicts a spiral path before exiting through the rotor inner radius (Fig. 1).

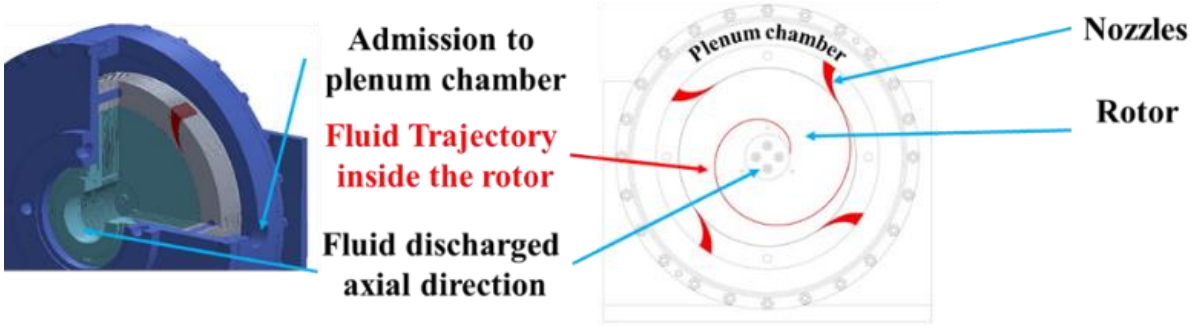


**Figure 1:** Tesla turbine schematic

### 2.1 Two-dimensional model

A two-dimensional numerical model for the assessment of the fluid dynamics of the Tesla turbine rotor was developed in EES environment (Klein and Nellis, 2012). The model hypothesizes the fluid as real and compressible with steady and viscous flow. The body forces are assumed to be negligible compared to the viscous forces along the radial and tangential directions. These hypotheses lead to a simplified formulation of the Navier-Stokes equations in cylindrical coordinates; the full set of equations is available in (Talluri *et al.*, 2018; Manfrida and Talluri, 2019).

The present model was solved on the basis of the assumption of a parabolic axial velocity profile corresponding to fully developed laminar flow (Guha and Sengupta, 2014; Talluri *et al.*, 2018). This assumption is justified as the most common operating flow regime of a Tesla turbine is in the laminar region. However, the control coefficients of the axial velocity profile were adjusted to account for transitional conditions occurring in the entry region.

The reduced $\theta$ and $r$ momentum equations were obtained and defined in the EES software by using a step forward method (centred finite difference):

$$\frac{\partial w_\theta}{\partial r} = -\frac{10}{a}\Omega - \left(\frac{60\nu}{w_r a b^2} + \frac{1}{r}\right) \cdot w_\theta \tag{1}$$

$$\frac{1}{\rho}\frac{dp}{dr} = -w_r \frac{\partial w_r}{\partial r} \cdot \frac{a^2}{30} + \Omega^2 r + 2\Omega w_\theta \frac{a}{6} + \frac{w_\theta^2}{r} \cdot \frac{a^2}{30} - \nu w_r \cdot \frac{2a}{b^2} \tag{2}$$

Where: $w$ is the relative velocity [m/s], $r$ is the radius [m], $\rho$ is the density [kg/m$^3$], $\Omega$ is the rotational speed [rad/s], $b$ is the rotor width [m] and $a$ is the control coefficients of the axial velocity profile.
High values of the coefficient $a$ determine pronounced parabolic distributions, typical of fully developed laminar flows, while low values of that parameter are related to transitional and laminar flows, characteristic of the entry region. It was evaluated that in the entry region the correct value of the $a$ coefficient is around 4, as there the flow is not fully developed (Ciappi *et al.*, 2019).

### 2.2 3-D CFD model

In order to assess the interaction between stator and rotor as well as to analyse the sources of inefficiency occurring in the gap between them, a separated approach does not provide accurate results. Therefore, a coupled stator–rotor simulation was set.
In Fig. 2, the fluid domain of the Tesla turbine and two close-ups of the mesh are shown. In order to speed up computations, the simulations were performed on a computational domain consisting of a portion of the plenum chamber, one of four static nozzles, the gap between the stator and the rotor and a 90° sector of the rotor, representing ¼ of a single rotor disk passage.
Several different meshes with a number of elements in the range from 0.4 to 3 million were examined in order to assess the mesh independency of computational results. With the aim to achieve the optimum grid size as a compromise between accuracy and computational time, a 2 million elements mesh was finally selected by fulfilling the minimum change of rotor inlet tangential velocity of $1 \cdot 10^{-3}$ m/s.
In the solver settings, the Navier–Stokes equations were discretised with second scheme for pressure and second order upwind for density, momentum, energy, turbulent kinetic energy and the SIMPLE scheme was used to relate velocity and pressure corrections. To compute the variable gradients, the least–squares cell–based methods was applied. The turbulence closure was done both with the laminar model and the Langtry–Menter transitional shear stress transport model (SST) with second order discretisation.
A velocity inlet boundary was imposed at the inlet of the plenum chamber and an outlet pressure boundary was imposed at rotor outlet. Periodicity boundary condition was assigned to the side walls of the ¼ of the cylindrical domain. Adiabatic wall condition was set. The rotation feature of the rotor was applied by setting frame motion with constant frequency of rotation in the rotor cell zone.

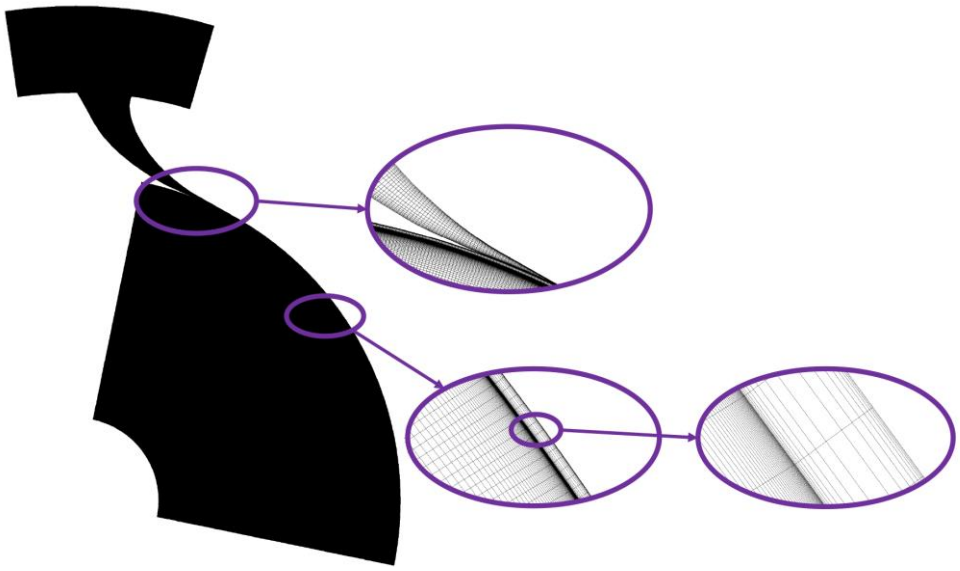

**Figure 2:** Three–dimensional computational domain of the Tesla turbine

## 3. RESULTS

The numerical analysis of the Tesla turbine with coupling of stator and rotor were performed with R1233zd(E) as working fluid. The values of the inlet/outlet boundary conditions are resumed in Table 1.

**Table 1:** Boundary conditions for coupled stator–rotor analysis

| rpm | Total inlet pressure [Pa] | Total inlet temperature [°C] | Static outlet pressure [Pa] | Static outlet temperature [°C] |
|---|---|---|---|---|
| 3000 | 493133 | 72.66 | 311778 | 66.72 |

### 3.1 Rotor flow interpretation

In Fig. 3, the contours of the static pressure, static temperature, tangential velocity and radial velocity are shown. Partial admission effects are evident when analysing the temperature trend in Fig. 3b. The temperature distribution inside the rotor is not uniform, but it displays clearly four different temperature regions, which are due to the spiral trajectories of the fluid from the four nozzle admissions. Nonetheless, the difference in temperature between one stream and the other is almost negligible (local maximum difference of 5°C); as it does not influence the results of power calculation. As expected, the highest temperature drop occurs at the nozzle exit, while the temperature drop in the rotor is very small, as is the relative total pressure drop. Indeed, the relative total pressure drop in the rotor is of about 30 kPa, which is a very small portion of the total pressure drop of about 180 kPa, which is mainly produced by the stator (146 kPa), visible in Fig. 3a. In this case, the Tesla turbine works similarly to an action turbine, where the relative total pressure drop is almost entirely converted in velocity in the nozzles. The radial velocity is steadily increasing towards the centre, which is determined by the continuity equation and by the decreasing passage section. Close to the nozzle exit, a peak of radial velocity is present. This peak does not globally influence the performance results of the simulations, but it has to be taken into account as the discrete number of nozzles affects the flow field of the turbine.
The tangential velocity behaviour presents a trend in agreement with the literature models, that consider the isolated rotor flow solution (Carey, 2010; Guha and Sengupta, 2014). At first, the viscous force effects cause a considerable reduction of tangential velocity, while when the flow approaches the inner radii, the angular momentum effect prevails, resulting in the fluid velocity increase, and thus to a lower transfer of momentum to the walls.

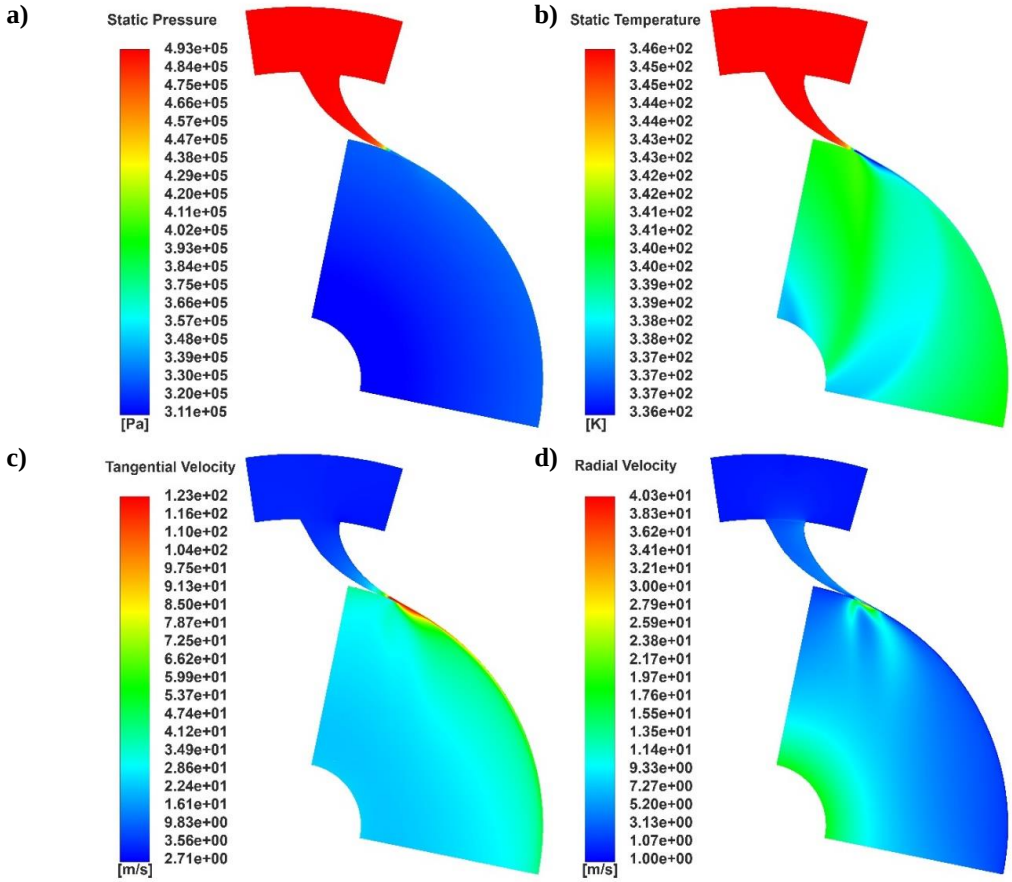


**Figure 3:** Mid-plane contours of a) static pressure [Pa] b) static temperature [K] c) tangential velocity [m/s] d) radial velocity [m/s] at 3000 rpm for the 3-D CFD model

### 3.2 Flow distortion at rotor inlet

In order to assess the effects of the interaction between stator and rotor, as well as to understand the influence of the gap between them, five reference sections were selected within the domain of the developed analysis. As displayed in Fig. 4, the sections correspond to: $s_1$ (throat), $s_2$ (stator outlet), $s_3$ (stator-rotor gap inlet), $s_4$ (stator-rotor gap outlet) and $s_5$ (rotor inlet).
The distortion of the flow is highlighted by taking the mass weighted average of the main fluid dynamics variables in sections from $s_1$ to $s_5$.

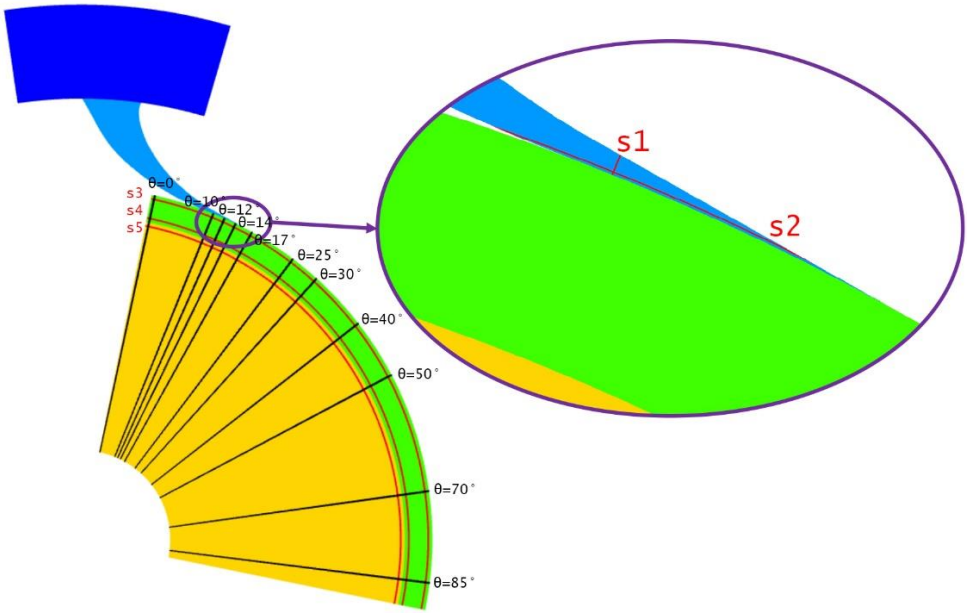


**Figure 4:** Scheme of the reference sections with highlight of sections

As can be noted in Fig. 5, a rapid decrease of the total pressure due to a drastic decrease of the absolute velocity magnitude is present in the gap between stator and rotor ($s_3$-$s_4$). Conversely, as it was expected, the static pressure of sections $s_3$ and $s_4$ is about the same. Indeed, the conversion occurring inside the gap, can be treated as a para-isenthalpic expansion process (like a process valve), conserving total enthalpy and reducing the pressure due to total pressure expansion losses. Along with a reduction of total pressure, the viscous flow effects and the flow entrainment in the gap produce an increase of the static temperature at rotor inlet of about 2-3 K, due to the drastic velocity reduction. Another important parameter, which needs to be discussed, is the radial velocity. The fluctuating trend is due to an adjustment of flow direction: the flow proceeding from nozzle exit to rotor inlet progressively loses its tangential behavior.

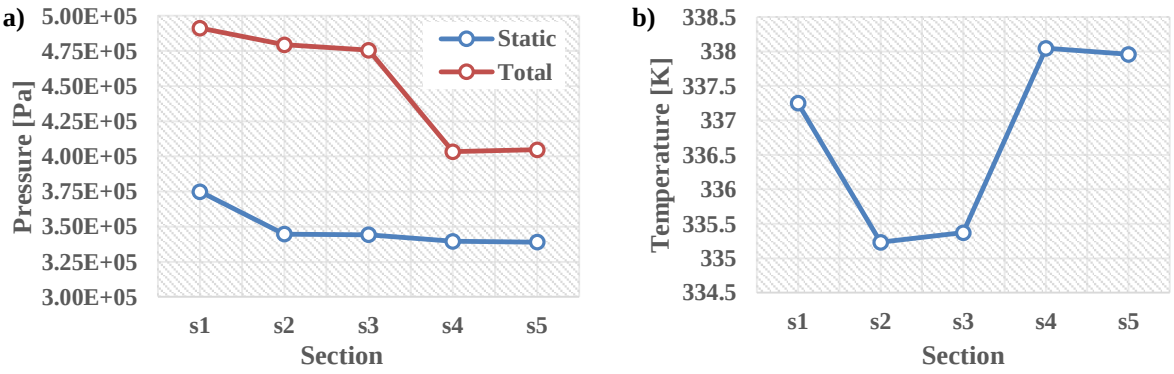

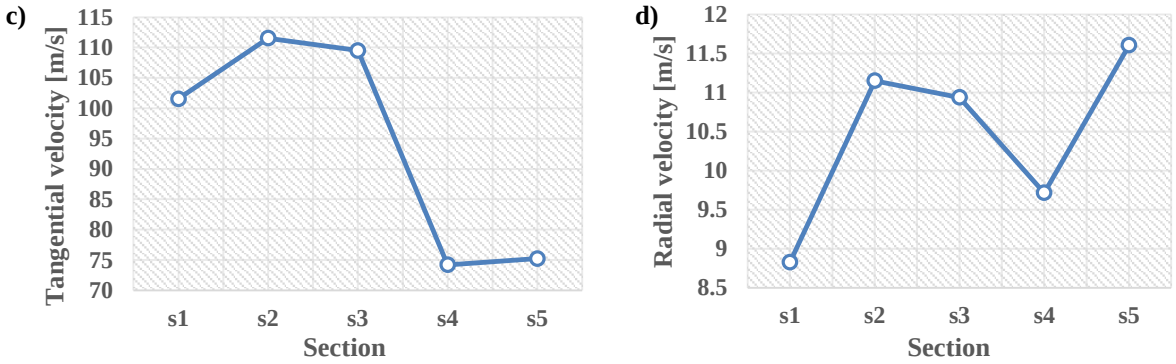


**Figure 5:** Mass-weighted values of a) Pressure, b) Temperature, c) Tangential velocity, d) Radial velocity at each defined section

After analyzing the most significant thermo-fluid dynamics variables through the averaged values calculated in sections $s_1$ to $s_5$, it is important also to examine the trend of the same variables along the tangential direction, in order to properly assess the effects of the gap and especially the influence of partial admission.

This last is evident between $\theta = 10°$ and $\theta = 17°$ (Fig. 6). The total pressure and flow velocities present high peaks in the region of the nozzle exit; also the temperature in correspondence to the velocity field distortion presents a significant drop in the same region, as expected. The distribution of static pressure is less influenced by the partial admission, while the tangential velocity presents a highly distorted trend, which become homogeneous only after a few equivalent diameters inside the rotor (Fig. 3).

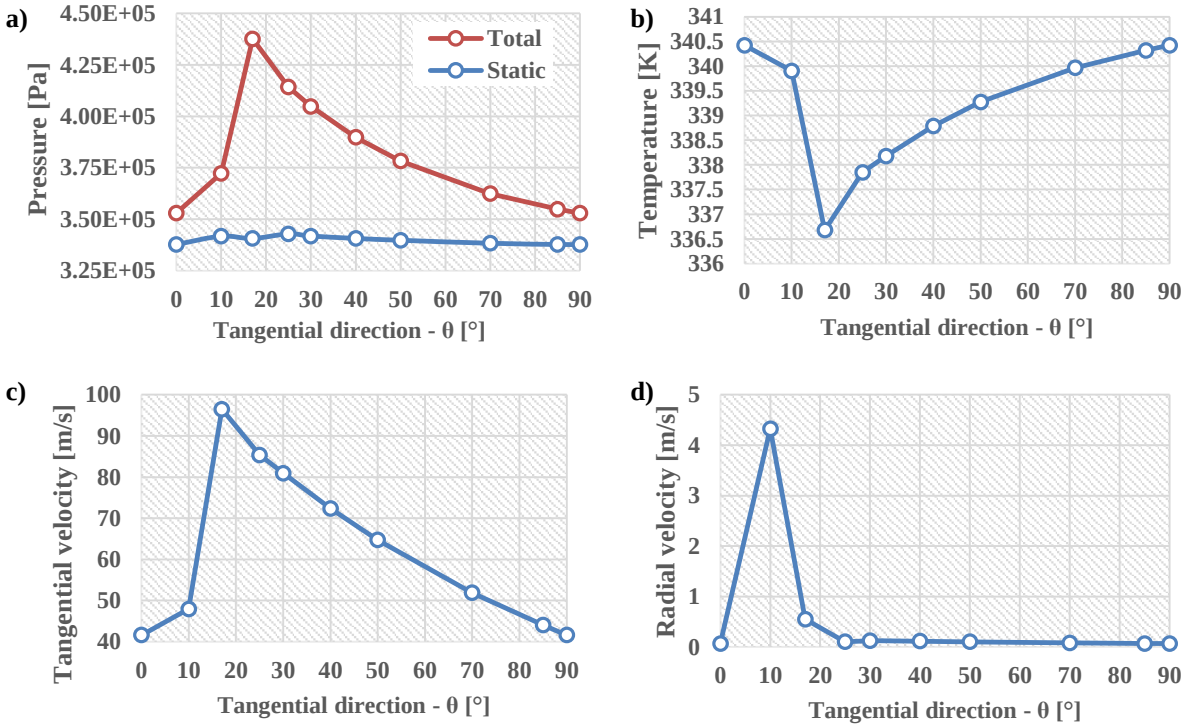


**Figure 6:** Mass Weighted values of a) Pressure, b) Temperature, c) Tangential Velocity, d) Radial velocity along tangential direction

Furthermore, from the visualization of the contour plot of the tangential velocity (Fig. 7), an asymmetric flow at rotor inlet and an intensified effect in the admission region is noticeable, while proceeding far from the admission ($\theta$<10; $\theta$>25), the flow field become symmetric. These effects were expected due to the geometry of the machine, as each stator channel supplies a mass flow rate for two rotor channels. It can be noted in Fig. 7 for $\theta$=10° where half stator channel is presented together with a rotor channel. On the whole, the flow distortion seems to be very strong for a very limited part of the rotor (from $\theta$=10 to $\theta$=17), which is the part that is directly interacting with the stator; while the majority of rotor inlet

experiences a nearly homogeneous flow distribution.

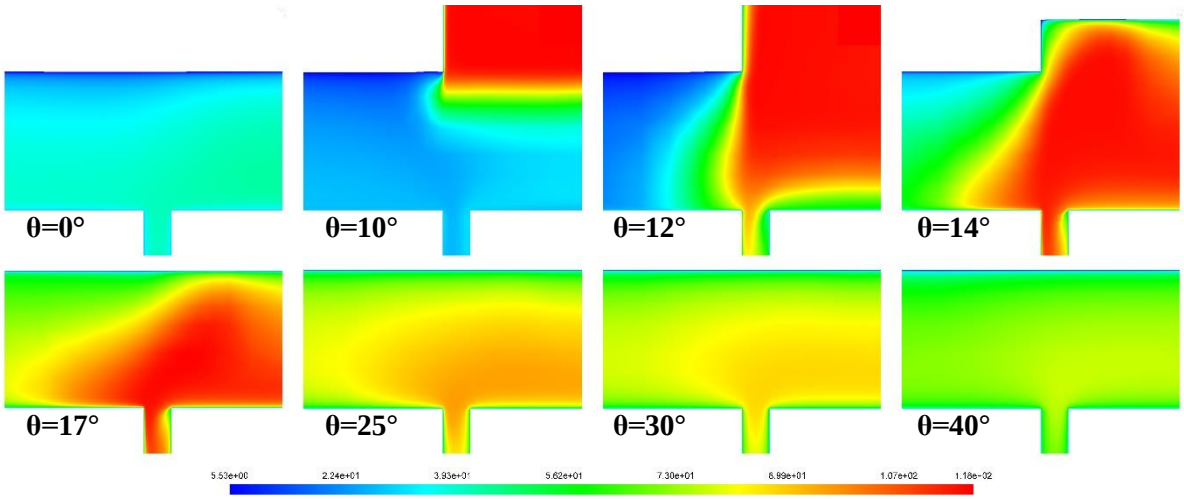


**Figure 7:** Contours of the tangential velocity at various angular positions ($\theta$)

### 3.3 Performance assessment

Finally, a comparison in terms of power and efficiency is presented in Tab. 2 between the 3-D CFD results and the 2-D EES results. As can be noted from Tab. 2, the performance prediction between 2-D code and 3-D CFD is really close, both in terms of power and efficiency. Therefore, it can be stated that the distortion of the flow field does not considerably influence the performance of the turbine in terms of power and efficiency when mass weighted average values are considered.

**Table 2:** Comparison of the global results of the 2-D in-house and 3-D CFD models

| rpm | Total mass flow rate [kg/s] | Rotor efficiency | Turbine efficiency | Power per channel [W] | Total power [W] |
|---|---|---|---|---|---|
| | | | **2-D EES model** | | |
| 3000 | 0.242 | 0.51 | 0.29 | 9.57 | 574.3 |
| | | | **3-D CFD model** | | |
| 3000 | 0.242 | 0.50 | 0.28 | 9.52 | 571.3 |

## 4. CONCLUSIONS

A computational fluid dynamic assessment was carried out in order to evaluate the flow field and the performance of a Tesla turbine working with R1233zd(E). A 29% turbine efficiency for a 0.57 kW expander is confirmed. The analysis shows that partial admission effects are not negligible in the flow field region entering the Tesla turbine rotor. However, these effects do not affect significantly the machine performance in terms of power and efficiency. The physical reason is that an attenuation already occurs in the stator-rotor gap, and viscous effects in the rotor determine the rapid development of relatively homogeneous conditions. Consequently, the 3-D CFD calculations confirm that 2-D simulations of the isolated rotor are adequate to provide performance predictions.
The pivotal point of this research is the development of a coupled stator-rotor simulation of a Tesla turbine for ORC. The key outcomes may be summarized in the following way:

- Stator–rotor interaction simulations allowed understanding the flow features due to partial admission. Especially, temperature was found to be the variable most influenced by the flow distortion, developing streaks of different temperature in tangential direction.
- Stator–rotor coupled simulations carried out with 3-D CFD do not affect the prediction of work and efficiency, if compared to simulations done with the 2-D EES in-house tool on the rotor. Nonetheless, they allow for a more detailed investigation of the critical points of the expander, such as the nozzle outlet operation and the influence of the gap.
- The results of the stator–rotor simulations in ANSYS Fluent model and 2-D EES in–house code were compared showing good matching of the performance prediction.

## NOMENCLATURE

**Latin symbols**

| | | |
|---|---|---|
| a | coefficient | (-) |
| b | channel width | (m) |
| $\dot{m}$ | mass flow rate | (kg/s) |
| p | pressure | (Pa) |
| r | radius | (m) |
| v | absolute velocity | (m/s) |
| $\dot{W}$ | power | (W) |
| w | relative velocity | (m/s) |

**Greek symbols**

| | | |
|---|---|---|
| $\eta$ | Efficiency | (-) |
| $\rho$ | Density | ($kg/m^3$) |
| $\Omega$ | Rotational velocity | (rad/s) |
| $\nu$ | Kinematic viscosity | ($m^2/s$) |

**Subscript**

| | |
|---|---|
| r | Radial |
| $\theta$ | Tangential |
| is | Isentropic |
| su | Supply |

## REFERENCES


Carey V P, 2010, Assessment of Tesla Turbine Performance for Small Scale Rankine Combined Heat and Power Systems, *Journal Eng. Gas Turbines Power*, 132: 1–8.

Ciappi L, Fiaschi D, Niknam P H, Talluri L, 2019, Computational investigation of the flow inside a Tesla turbine rotor, *Energy*, 173: 207-217.

Dumont O, Parthoens A, Dickes R, Lemort V, 2018, Experimental investigation and optimal performance assessment of four volumetric expanders (scroll, screw, piston and roots) tested in a small–scale organic Rankine cycle system, *Energy*, 165: 1119–1127.

Guha A, Sengupta S, 2014, The fluid dynamics of work transfer in the non–uniform viscous rotating flow within a Tesla disc turbomachine, *Physics of Fluids*, 26: 1–27.

Hoya G P, Guha A, 2012, The design of a test rig and study of the performance and efficiency of a Tesla disc turbine, *Proc. IMechE, Part A: Journal of Power and Energy*, 223: 451–465.

Klein SA, Nellis GF, 2012, *Mastering EES*, f-Chart software.

Krishnan V G, Romanin V D, Carey V P, Maharbiz M M, 2013, Design and scaling of microscale Tesla turbines, *Journal of Micromechanics and Microengineering*, 23.

Lampart P., Jedrzejewski L., 2011, Investigations of aerodynamics of Tesla bladeless microturbines, *Journal of Theoretical and Applied Mechanic*, 49, 2: 477–499.

Lemort V., Legros A., 2016, Positive displacement expanders for Organic Rankine Cycle systems, *In:* Macchi M. and Astolfi M., *Organic Rankine Cycle (ORC) Power Systems, Technologies and Applications*, 1st Edition, Woodhead Publishing, Elsevier.

Manfrida G., Pacini L., Talluri L., 2018. An upgraded Tesla turbine concept for ORC applications, *Energy*, 158: 33–40.

Manfrida G., Talluri L., 2019. Fluid dynamics assessment of the Tesla turbine rotor, *Thermal Science*, 23: 1-10.

Qiu G, Liu H, Riffat S, 2011, Expanders for micro-CHP systems with organic Rankine cycle, *Applied Thermal Engineering*, 31: 3301-3307.

Rice W., 1965, An analytical and experimental investigation of multiple-disk turbines, *ASME Journal of Engineering for Power*, 87: 29-36.

Schosser C., Lecheler S., Pfizner M., 2014, A test rig for the investigation of the performance and flow field of Tesla friction turbines, *Proceedings of ASME Turbo Expo 2014: Turbine Technical Conference and Exposition*, Dusseldorf.

Schosser C, Pfitzner M, 2015, A numerical study of the three–dimensional incompressible rotor airflow within a Tesla turbine, *Conference on Modelling Fluid Flow (CMFF'15)*, Budapest.

Song J., Gu C.W., Li X.S., 2017, Performance estimation of Tesla turbine applied in small scale Organic Rankine Cycle (ORC) system, *Appl. Therm. Eng.*, 110: 318–326.

Song J, Ren X D, Li XS., Gu CW., Zhang MM., 2018, One-dimensional model analysis and performance assessement of Tesla turbine, *Applied Thermal Engineering*, 134: 546-554.

Talluri L., Fiaschi D., Neri G., Ciappi L., 2018, Design and optimization of a Tesla turbine for ORC applications, *Appl. Energy*, 226, 300–319.